The Fifth International Workshop on Micro and Nanotechnology for Power Generation and Energy Conversion Applications
PowerMEMS 2005
Nov. 28-30, 2005
Takeda Hall, The University of Tokyo, Tokyo, Japan

MEMS Acoustic Energy Harvester

Stephen B. Horowitz, [1] Mark Sheplak, [2] Louis N. Cattafesta III, [2] and Toshikazu Nishida [1]
[1]Dept. of Electrical and Computer Engineering, [2]Dept. of Mechanical and Aerospace Engineering
Interdisciplinary Microsystems Group
University of Florida, Gainesville, Florida 32611-6200, U.S.A.
Tel (352)392-6774, Fax (352) 392-8671, E-mail nishida@ufl.edu

Abstract

This paper presents preliminary results towards the development of a micromachined acoustic energy harvester for aeroacoustic applications. The acoustic energy harvester employs a circular, piezoelectrically active diaphragm for acoustical-to-mechanical and mechanical-to-electrical transduction. Lumped element modeling, design, fabrication, and characterization of a micromachined acoustic energy harvester prototype are presented. Results indicate a maximum output power density of 0.34 $\mu W/cm^2$ at 149 *dB SPL* using currently fabricated devices and suggest a possible output power density, for this design, of 252 $\mu W/cm^2$ with improved fabrication conditions.

Keywords: piezoelectric, microfabricated, energy reclamation, lead-zirconate titanate

1 INTRODUCTION

We report progress towards a microelectromechanical systems (MEMS) acoustic energy harvester. To enable wireless sensor nodes that are not dependent on replaceable batteries, power needs to be collected locally from the environment. Most energy harvesting efforts have focused on vibrations [1], ambient light [2], and temperature gradients [3] as the environmental energy sources. Acoustic energy is another potential energy source in certain applications. Acoustic energy harvesting (AEH) has been demonstrated recently using a mesoscale Helmholtz resonator machined in aluminum (dimensions: 24.8 *mm* diameter, and 16.1 *mm* length with a 20.2 *mm* diameter circular piezoelectric patch), delivering 25 *mW* to a resistive load at 152 *dB* (ref. 20 μPa) sound pressure level (SPL) [4, 5]. This acoustic energy may be used to locally power a wireless active liner for suppression of engine noise in turbofan engine nacelles, where noise levels typically reach upwards of 150 *dB* [5]. However, the density and proximity of Helmholtz resonators in the active liner may preclude the use of mesoscale fabrication approaches.

2 THEORETICAL BACKGROUND

The goal of this work is the development of a silicon micromachined AEH, including lumped element modeling, scaling analysis, design, fabrication, and characterization. Figure 1 gives a schematic of the overall system. Incident acoustic waves impinge on the AEH, shown in the dashed circle. A fraction of the acoustic energy is transferred to the harvester where it is converted into an ac voltage, rectified, and stored. In one approach, shown in Figure 2, the AEH utilizes a conventional Helmholtz resonator (HR) as a tuned, 2nd order resonator for pressure amplification.

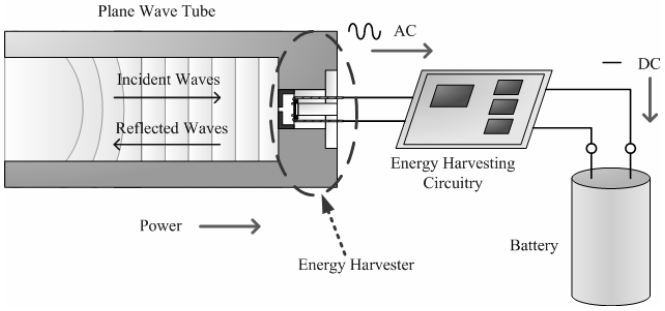

Figure 1. Schematic of overall acoustic energy harvester.

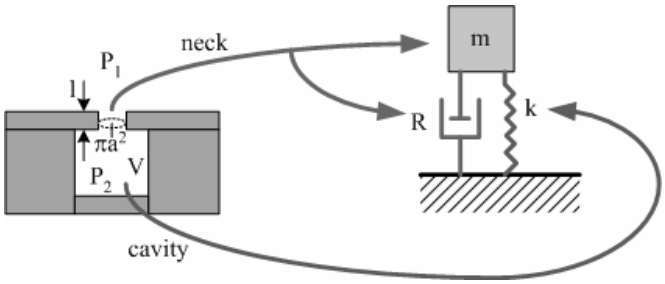

Figure 2. Lumped model of the Helmholtz resonator.

The distributed HR may be lumped in terms of a mass, *m*, stiffness, *k*, and damper, *R*, provided the quasi-static assumption is valid. An electromechanical HR (EMHR) is formed by replacing the rigid backplate of the HR with a composite diaphragm with a piezoelectric ring (Figure 3).

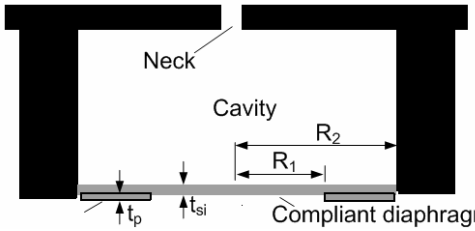

Figure 3. Electromechanical Helmholtz resonator.

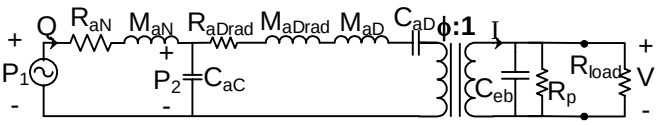

Figure 4. Complete equivalent circuit for EMHR AEH.

An equivalent circuit [5] of the EMHR consists of the mass-spring-damper equivalent of the HR (M_{aN}, C_{aC}, R_{aN}) where C_{aC} is the acoustic cavity compliance, augmented with the diaphragm lumped mass, M_{aD}, and compliance, C_{aD}, and radiation resistance, R_{aDrad}, and mass, M_{aDrad}, and a transformer representing the piezoelectric transduction ratio, ϕ, and the electrical blocked capacitance, C_{eb}, dielectric loss resistance, R_p, and load resistance, R_{load}, as shown in Figure 4.

To analyze the scaling of the AEH, the acoustic energy harvester efficiency is calculated for a range of dimensions. A representative example is plotted in Figure 5 for an assumed incident pressure of 1 *Pa* (94 *dB* referenced to 20 μPa). Two resonances are observed in the efficiency, defined as the ratio of the output electrical power to input acoustic power. The efficiency of the composite plate alone (without HR) exhibits a single peak at the diaphragm resonance (3677 *Hz*) while the efficiency of the coupled EMHR has two peaks, one due primarily to the HR and the other due primarily to the diaphragm.

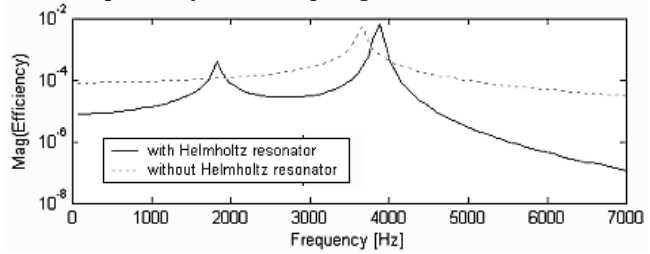

Figure 5. Simulated magnitude of acoustic energy harvester efficiency. **(***L=3.18mm, a=2.36mm, V_{cav}=1950 mm^3, t_{si}=3um, R_2=1.95mm, R_1=1.85mm).*

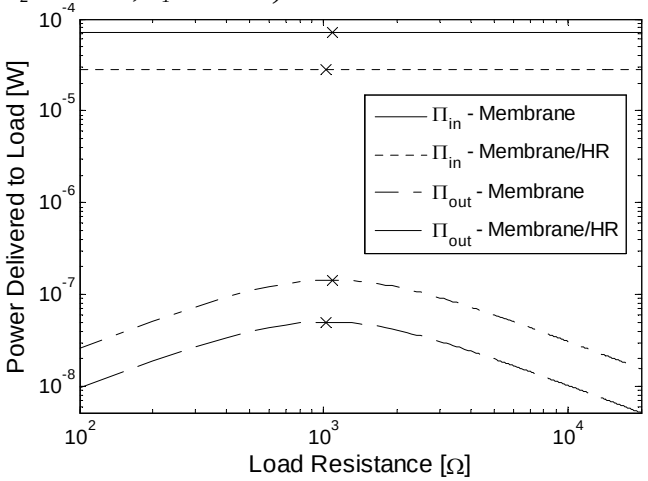

Figure 6. Simulated output power versus load resistance. (f_{HR}=3889 *Hz*, f_{mem}=3677 *Hz*, *P*=1 *Pa (94dB)).*

The output power is simulated as a function of load resistance when the composite plate alone (membrane) and the EMHR (membrane/HR) are excited at their respective resonant frequencies, 3677 *Hz* and 3889 *Hz*, showing a peak when a load resistance equal to the magnitude of the Thévenin impedance is chosen (Figure 6).

3 FABRICATION AND PACKAGING

The fabrication process flow (Figure 7) utilizes the epitaxial silicon layer of a silicon-on-insulator (SOI) wafer as the primary mechanical material of the diaphragm and a ring shaped layer of lead zirconate titanate (PZT) as the piezoelectric material.

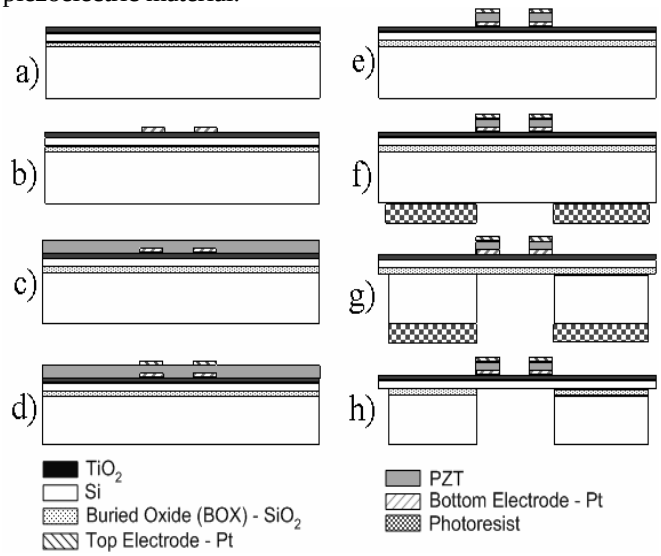

Figure 7. Concise process flow for the MEMS acoustic energy harvester. a) Deposit 100 *nm* of Ti and oxidize to TiO_2. b) Deposit and liftoff Ti/Pt (40/180 *nm*). c) Spin PZT 52/48 solution & pyrolize (4 layers for 267 *nm* total). d) Deposit and liftoff Pt (180 *nm*). e) Wet etch PZT in 3:1:1 of $(NH_4)HF_2$/HCl/DI water. f) Spin & pattern thick photoresist on back. g) Deep reactive ion etch to buried oxide layer. h) Ash resist and wet etch backside to remove the buried oxide.

A fabricated AEH chip, shown in Figure 8(a), was packaged as shown in Figure 8(b) and mounted in a 1"x1" acoustic plane wave tube that was driven acoustically by a BMS 4590P coaxial compression driver.

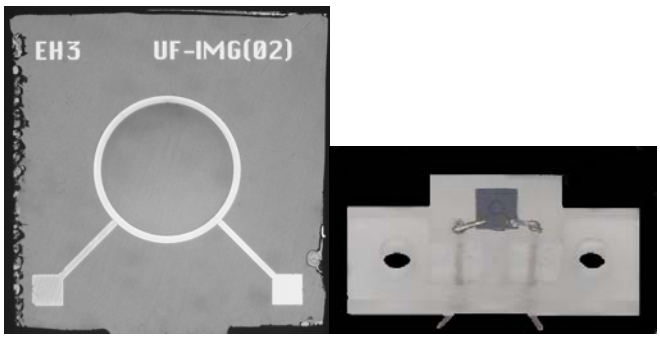

a) b)

Figure 8. (a) Fabricated MEMS EMHR AEH chip. (b) Packaged device.

4 EXPERIMENTAL SETUP AND RESULTS

Using a Stanford Research Systems SRS785 Dynamic Signal Analyzer, the AEH resonant frequency values were obtained. The SRS785 recorded 500 averages of 800 frequency bins over a frequency span of 25.6 *kHz*. The measured resonant frequencies are 13.568 *kHz* and 5.232 *kHz* for two MEMS AEH designs, Device 1 and Device 2 with geometries as defined in Table 1 .

Table 1. Geometric properties of tested devices.

Device	$R_1\ [\mu m]$	$R_2\ [\mu m]$	$t_p\ [\mu m]$	$t_{si}\ [\mu m]$
1	1115	1200	0.267	3
2	1685	1800	0.267	3

Once the resonant frequencies were determined, the source was changed to a sinusoidal signal at the resonant frequencies for the respective devices. The output voltage was then measured while the load resistance was varied from 46.4 Ω to 1.003 $M\Omega$. The output power was then calculated by

$$\Pi_{out} = V^2 / R_{load} \ , \qquad (1)$$

and the results were then plotted as shown in Figure 9. The figure is overlaid with the theoretical values for comparison. The experimentally determined resistance for maximum power for both of these devices was found to be 982.9 Ω .

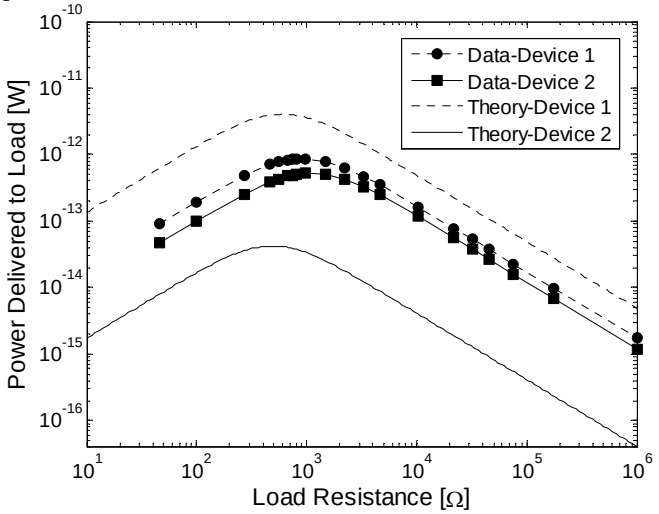

Figure 9. Measured power delivered to the load versus load resistance, compared to theory.

Using the resonant frequency and load resistance measured previously, the input signal was steadily increased in amplitude while the output voltage was measured. The power was then calculated based on the voltage and resistance measurements, again according to Eq. (1). The output voltage was found to be linear up to 125 *dB* for device 1 and up to 133 *dB* for device 2 and was seen to range between 22 μV and 4.6 mV (Figure 10).

The power density was then calculated based on a square unit cell with lateral dimensions equal to the diameter of the diaphragm. The resulting values are shown in Figure 11 and are again overlaid with theoretical values. Note from the graph that the maximum power density measured was around 0.34 $\mu W/cm^2$ for 149 *dB* , which is considerably lower than the available acoustic power density, 80 mW/cm^2 at the acoustic pressure of 149 *dB* .

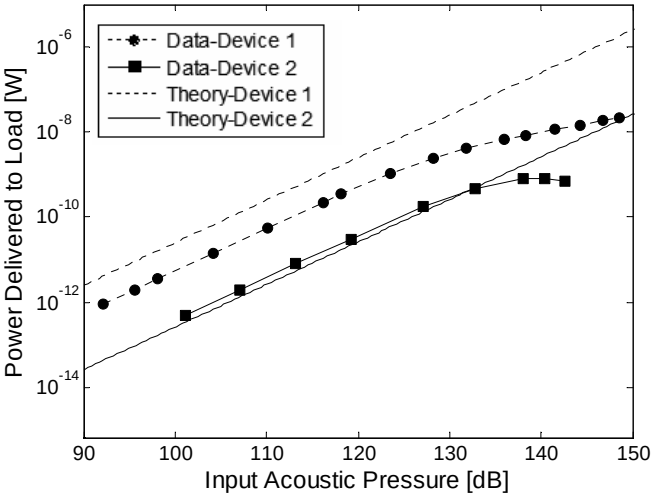

Figure 10. Measured power delivered to load as a function of acoustic pressure, compared to theory.

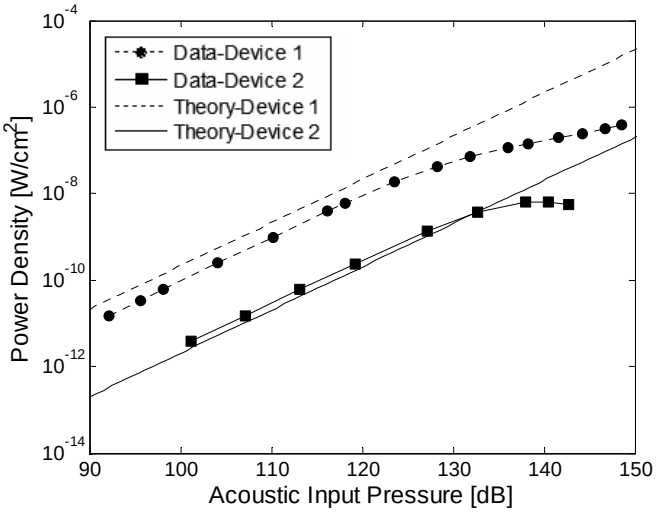

Figure 11. Measured power density delivered to load as a function of acoustic pressure, compared to theory.

The efficiency was then calculated according to

$$\eta = \Pi_{out} / \Pi_{in} \qquad (2)$$

for each of the devices. The efficiency was found to be fairly constant near 0.012 % for Device 1 in the linear regime and 4×10^{-4} % for Device 2 in the linear regime. A question then arises regarding the origin of the low efficiency and whether improvements in either the manufacturing or design of the devices could improve the efficiency, and thereby the output power. Several issues were

faced during the fabrication process that limited the efficiency of the devices. First, the materials and processes led to a large residual stress in several layers of the device, most notably the titanium dioxide. The effect of this large tensile stress, σ_{TiO_2}, is twofold: (1) an alteration of the deflection mode shape of the devices and (2) a large, non-linear, initial deflection of the diaphragm. It is estimated that the power density is decreased by a factor of 4.3 over the ideal zero-stress case.

A second issue arising from the fabrication was overhanging metal on the electrodes that created short circuits under high electric fields. This field limitation imposed a maximum poling voltage and limited the resulting polarization. The poling limitation reduced the power density by a factor of 24.6 versus a typically poled device.

The final fabrication issue concerns the piezoelectric material and the process by which it is deposited on the wafer. The particular sol-gel technique that was employed produces a typical d_{31} of -50 pC/N, whereas other variations of the sol-gel process as well as techniques such as sputtering can produce a film with a d_{31} of -120 pC/N. The output power density was reduced by a factor of 2.8 as a result of the lower value of d_{31} as compared to other reported PZT thin films.

Finally, if the quality factor, Q, were increased from a measured value of 10 for Device 2 to a more typical value of 25, then the output power density would increase by a factor of 2.5.

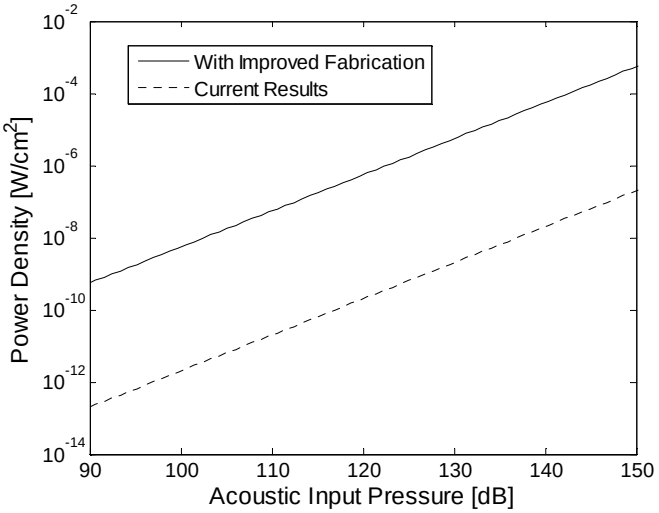

Figure 12. Currently achievable power density for Device 2 and potentially achievable power density under improved fabrication conditions.

Provided that all of the other sources of inefficiency are addressed, including the PZT material quality, the poling capability, and the residual stress, the overall power density would increase by a factor of 740. The resulting power density curve is shown in Figure 12, overlaid with the currently achievable results. With these improvements, at 149 dB, the output power density would be on the order 252 $\mu W/cm^2$. Additionally, the individual contributions to this improvement are given in Figure 13, clearly showing the prominent role of improving the piezoelectric coefficient, d_A, to the overall results where d_A is an effective piezoelectric coefficient that takes into account the mode shape and boundary conditions.

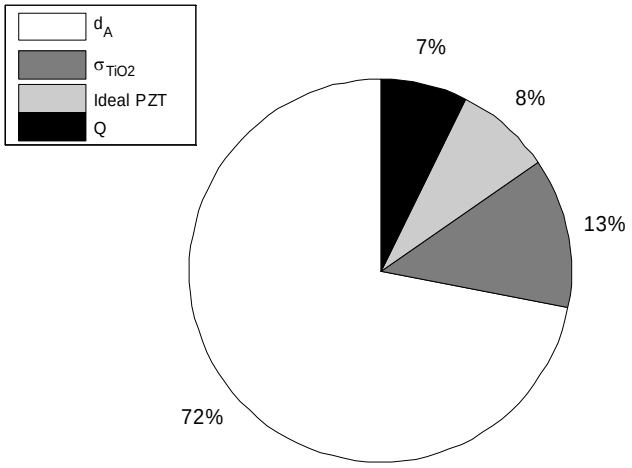

Figure 13. Breakdown of the individual contributions to the overall improvement achievable under improved fabrication conditions.

5 CONCLUSION

The development of an acoustic energy harvester for aeroacoustic applications that employs a micromachined piezoelectric diaphragm was presented. Theoretical aspects of the design were addressed, along with a brief overview of the fabrication process and packaging scheme. Preliminary energy harvesting experiments indicate a power density of 0.34 $\mu W/cm^2$ for an acoustic input of 149 dB. Furthermore, calculations indicate a potentially achievable power density of 252 $\mu W/cm^2$ at 149 dB SPL using the same design but under improved fabrication conditions.

6 REFERENCES

[1] S. Roundy, P. K. Wright, and J. Rabaey, *Computer Comm.* 26, pp. 1131-1144, 2003.

[2] B. A. Warneke et al., Proc. IEEE Sensors '02, pp. 1510-1515, 2002.

[3] M. Strasser et al., Proc. Transducers '03, pp. 45-48, 2003.

[4] S. Horowitz, A. Kasyap, D. Johnson, T. Nishida, K. D. T. Ngo, M. Sheplak, and L. Cattafesta, AIAA 1st Flow Control Conference, AIAA paper 2002-2702, 2002.

[5] R. Taylor, F. Liu, S. Horowitz, K. Ngo, T. Nishida, L. Cattafesta, and M. Sheplak, Proc. ACTIVE '04, Paper A04-093, 2004.